RavinderReddyButreddy, et. al. International Journal of Engineering Research and Applications
www.ijera.com
ISSN: 2248-9622, Vol. 13, Issue 5, May 2023, pp. 29-41

RESEARCH ARTICLE OPEN ACCESS

Enhanced Structural and Electrochemical properties of spinel structured Ca doped nickel cobaltite nanoparticles synthesized by microwave hydrothermal method

Sathyanarayana Neelam[1], Rakeshkumar Thida[2],Shilpa Chakra Chidurala[2], Srinivasu Daripaalli[1], Ravinder Reddy Butreddy[1]*

[1]*Department of Physics, University College of Science, Osmania University, Hyderabad, Telangana, India.*
[2]*Centre for Nano Science and Technology, Jawaharlal Nehru Technological University, Hyderabad, Telangana, India.*
**Corresponding author*

ABSTRACT
An important parameter influencing the energy storage capacity in materials is specific capacitance (C_p). In this study, a series of $Ca_xNi_{1-x}Co_2O_4$ (x = 0.0 – 0.10) nanoparticles were prepared using microwave-hydrothermal (M-H) method. The obtained samples were sintered at 750^0C. All thesamples were characterized by using X-ray diffraction (XRD), Field Emission Scanning electron microscopy (FESEM), Fourier transform infrared (FTIR) and X-ray photoelectron spectroscopy (XPS). From X-ray diffraction studies, it is found that all the samples are cubic spinel with space group Fd-3m. The average lattice constant is varied in between 8.057(x = 0.0) to 8.090 (x = 0.06).The linear decrease in lattice constant is due to the difference in the ionic radii. The average grain size is in the range of 89 (x = 0.0) - 143 nm (x = 0.06) for all the samples. The grains are spherical in nature. The tetrahedral and octahedral absorption bands were observed at 577 cm^{-1} and 667 cm^{-1}respectively. The valence states of Ni^{2+}/Ni^{3+}, Co^{2+}/Co^{3+} and Ca^{2+} were confirmed from X-ray photoelectron spectroscopy. The electrochemical studies using CV and GCD were performed on all the samples. The high values of specific capacitance (C_{sp}), energy density (E_d) and power density(P_d) are found to be 355F g^{-1}, 10.9 Wh kg^{-1} and 235 W kg^{-1} respectively for the sample x = 0.06. Therefore, $Ca_{0.06}Ni_{0.94}Co_2O_4$ sintered at 750^0C shows good impedance and electrochemical properties which are useful for supercapacitor applications.

Keywords: Cubic spinel, microwave hydrothermal, specific capacitance, dielectric constant, electrochemical, supercapacitor.

Date of Submission: 25-04-2023 Date of acceptance: 05-05-2023

I. INTRODUCTION

Over the past few years, super capacitors have been extensively used in potential applications as energy storage devices, because of their high power density, long cycle life, safe operation and environment friendliness.Super capacitors are commonly used in systems that require high output power to be delivered in a short period of time, such as portable electronics, hybrid electric vehicles and number of micro devices [1]. Super capacitors have been even considered as an alternative to the batteries. However, because of their energy storage mechanism, the energy density of super capacitor is low compared to batteries [2]. Therefore to meet the next generation energy storage applications, the energy density of the super capacitors should be enhanced without scarifying its power density and long cycle life,various techniques have been developed to increase the energy density of super capacitors [3]. According to the equation $E=\frac{1}{2}CV^2$ [4], byincreasing the specific capacitance(C), and cell voltage (V), the energy density of super capacitor can be enhanced.According to reported study, the development a super capacitor with a battery-type faradic electrode and a capacitor-type electrode [5] can increase the energy density and voltage window of super capacitor. The principle performances of super capacitor like specific capacitance, cycling stability and rate capability were determined by the electrode material of super capacitor. Carbon-based materials, conductive polymers, and transition metal oxides (TMO) such as MnO_2, NiO, and Ca_2CO_3, etc, are commonly used as super capacitor electrode materials [6].The increased use of these nanoparticles in commercial products deserves a comprehensive analysis of their effect on the environment[7]. The carbon-based

materials have low specific capacitance because of the increase in electrical double layer capacitance (EDLC) from electrostatically stored surface energy at the interface of the electrode material [8, 9], whereas the conductive polymers show higher specific capacitance compared to carbon based materials, but suffer from low cycling efficiency [10]. When compared to carbon-made materials and conducting polymers, transition metal oxides (TMOs) exhibit higher specific capacitance because, during the process of charge and discharge, redox reactions take place on the surface of the material, and like in a battery electrode, energy transfer takes place between the electrolyte and electrode.

Therefore, different TMOs with different compositions and structures were synthesized to obtain high energy density and specific capacitance [11–13]. Especially transition metal oxides in the form of nanoparticles have been widely studied as an electrode material for super capacitor applications over the past two decades. Among various TMOs, $NiCo_2O_4$ has gained much importance as a super capacitor electrode material due to its low cost, high electronic conductivity, and availability in nature. It has been reported that 1-Dimensional Nickel Cobalt Oxide ($NiCo_2O_4$) nanowire films grown on Ni foam, because of itslarger specific capacitance, is considered to be one of the most potential candidates for the deposition of guest transition metal oxide materials such as $CoMn_2O_4$ [14], rGO [15], Co_3O_4 [16], MnO_2 [17], and $NiCo_2O_4$ [18]. Various studies have been done on $NiCo_2O_4$ composite nanoparticles. For example, a fabricated hybrid supercapacitor (SC) composed of a $NiCo_2O_4$-ITO anode and a graphite-ITO cathode delivered a specific capacitance of around 235 F g^{-1} in KOH solution [19]. The specific capacitance of nanostructured nickel cobalt oxides as supercapacitor electrodes in the aqueous medium KOH was reported to be 249.8 F g^{-1} at a current density of 0.5 A g^{-1} [20]. The specific capacitance of 112 F g^{-1} was reported for hierarchical mesoporous $NiCo_2O_4$-MnO_2 core shell nanowire arrays on nickel foam for an aqueous asymmetric supercapacitor [21]. At a current density of 0.67 Ag^{-1}, the nanocomposite films of nickel cobalt oxide and reduced graphene oxide exhibited a specific capacitance of 127 F g^{-1} [22]. We demonstrated the design and synthesis of Ca doped $NiCo_2O_4$ in hydrothermal deposition method and studied itsstructural, electrical, and electrochemical properties using various characterization techniques in this study.

II. EXPERIMENTAL METHODS

Nickel nitrate (Ni $(NO_3)_2.6H_2O$), Cobalt nitrate (Co $(NO_3)_2.6H_2O$) and Calcium nitrate ($Ca(NO_3)_2.6H_2O$) sodium hydroxide (NaOH) were purchased from Sigma Aldrich chemicals Pvt. Ltd, Bangalore, India. All the above chemicals were used without any further purification.In this present study, Ca substituted $NiCo_2O_4$ (NCO) nanocrystalline powder particles with the compositional formula $Ca_xNi_{1-x}Co_2O_4$ (x = 0.0, 0.02, 0.04, 0.06, 0.08, and 0.10) were prepared using the microwave hydrothermal (MH) method. The MH method has the characteristics of fast heating speed, sensitive reaction, and a uniform heating system so that it prepares nanoparticles with a narrow particle size distribution with uniform morphology. All the chemicals were weighed stoichiometrically in 30 ml of doubly distilled water and mixed well to prepare the molar solution. The prepared solution is stirred for 30 minutes on a magnetic stirrer until a homogeneous mixture is formed; during stirring, NaOH pellets are added to maintain a proper pH. Then the solution was transferred into autoclaves and placed in the CEM MARSXPRESS 230/60 microwave digestion system for chemical reactions at 160 ^{0}C for 40 minutes and allowed to cool for 2 hours; the precipitate that was formed in the process was cleaned 5–6 times with deionized water and ethanol to remove impurities from the solution. The solution is then dried in an oven at 70 ^{0}C for 48 hours. An agate mortar and pestle were used to grind the samples into fine powder particles. The obtained samples were calcinated at 750^{0}C for 4 hours in a muffle furnace to remove the contaminants. KBR's hydraulic pressure machine was used to prepare the pellets of 10 mm diameter and 2–3 mm thickness; these pellets were sintered at 750 ^{0}C for 4 hours.

For the analysis of structure, crystalline size, particle size, and phase identification of the sample, XRD technique was used by PANalytical, Xpert powder diffractometer employing Cu -Kα (λ=1.5405 Å) radiation at a scanning rate of 80^0 min^{-1} from 2θ = 10^0 to 90^0. For the analysis of organic and inorganic compounds present in the sample, the FTIR technique was used by the PerkinElmer FTIR/DTGS instrument.FESEM with EDAX technique was carried out with FEI ApreoS and OXFORD X-Max instruments to study the morphology of the surface and analyze the chemical composition of the surface. To study the energy states of elements and their binding energy, XPS technique was used, for which we used the Thermo Scientific K-Alpha instrument.For the analysis of thermal behavior of samples, the DSC technique is used by the PerkinElmer DSC 8000 instrument. To study the electrical properties, conductivity technique is used, which is carried out by PSM 1700 Frequency Response Analyzer.

III. RESULTS AND DISCUSSION

Fig. 1 shows the X-ray diffraction peaks at different 2θ angles and their respective miller indices of Ca doped Nickel Cobalt Oxide with compositional formula $Ca_xNi_{1-x}Co_2O_4$(x=0.0, 0.02, 0.04, 0.06, 0.08, and 0.10). Sharp peaks observed at diffraction angles 19.0^0, 31.21^0, 36.86^0, 38.56^0, 43.10^0, 44.72^0, 55.54^0, 59.32^0, 62.63^0, 65.14^0, $75.10^0$and 77.11^0confirm the formation of crystalline structure of the sample. All the observed peaks were well matched with standard JCPDS card no (01-073-1702) of $NiCo_2O_4$spinel cubic Fd-3m phase. As the electron density of doped Ca^{+2} ions($4.63x10^{29}m^{-3}$) is higher than that of Ni^{+2} ions ($1.8x10^{29}$ m^{-3}), it was observed that, the peak intensity of diffracted peak increases with doping concentrationwhich was clearly observed for x=0.06. The lattice constant of prepared samples was calculated using Bragg's equation,

$$2d\sin(\theta) = n\lambda \quad \text{--------} (1)$$

where, ddenotes Inter planar spacing between lattice planes,λrepresentsthe wave length of X-rays (1.5405Å).

$$(1/d^2)= (h^2/a^2) + (k^2/b^2) + (l^2/c^2) \quad \text{--------}(2)$$

where, d represents inter planar spacing, (h, k, l) denotes miller indices and a, b, c are the lattice constants.

For cubic crystal a=b=c, and in this present study, the lattice parameter was observed as 8.090A^o. The peak observed at diffracted angles 65.14^0 and 77.11^0, with which miller indices (222) and (400)were matched with COD CIF file (00-900-6726) of cubic CaO with space group Fm-3m, indicates the existence of doped Ca in the sample. The diffracted peak observed at $44.82^0$with the miller indices (111) were matched with COD CIF file (00-901-1603) of cubic Ni with space group Fm-3m.

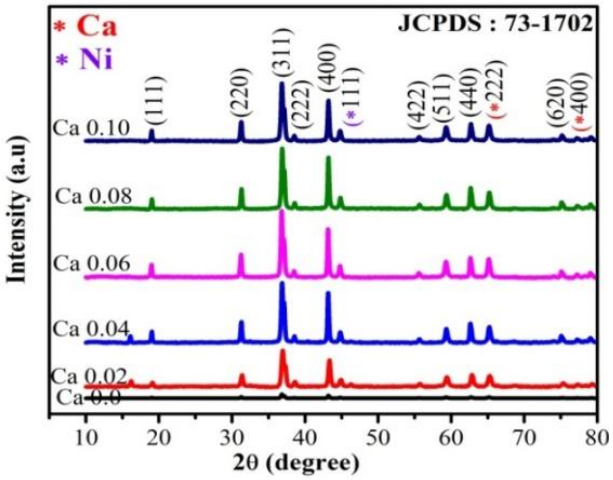

Fig. 1: XRD plot of pure and Ca doped $NiCo_2O_4$ NPs for x = 0.0, 0.02, 0.04, 0.06, 0.08, and 0.10.

The calculated lattice parameters of all the samples Ca doped $NiCo_2O_4$ with different doping concentration is shown in the Table 1.
The lattice constant of the samples was calculated by using the formula,

$$a = d\sqrt{(h^2+k^2+l^2)} \quad \text{-----} (3)$$

The average crystalline size of the samples was measured by using Debye Scherer's formula.

$$\langle D\rangle = k\lambda / \beta\cos\theta \quad \text{-----} (4)$$

where <D> denotes average crystalline size in nm, λ denotes wavelength of X-rays (1.5405Å), k represents the shape factor (k = 0.9), β represents the FWHM in radians; θ is the Bragg's angle of diffraction.

Table1: Values of Lattice parameter (a), Average crystalline size (D), and X-ray density (ρ) of $Ca_xNi_{1-x}Co_2O_4$ for x = 0.0, 0.02, 0.04, 0.06, 0.08, and 0.10 samples.

Sl.No.	**Ca doping, x**	**Lattice parameter $a = d\sqrt{(h^2+k^2+l^2)}$ (Å)**	**Crystal size $\langle D\rangle = 0.9\,\lambda / \beta\cos\theta$ (nm)**	**X-ray Density $\rho = 8M / Na^3$ (gcm^{-3})**
1	0.00	8.057	15.561	6.108
2	0.02	8.058	15.804	6.096
3	0.04	8.079	16.558	6.020
4	0.06	8.090	16.684	5.987
5	0.08	8.076	16.384	6.037
6	0.10	8.083	15.716	6.031

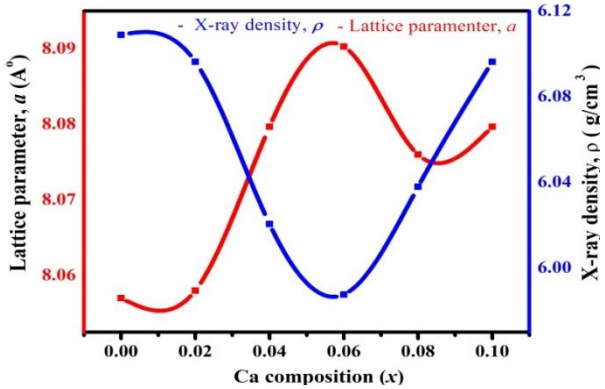

Fig.2: Plot drawn between variation of Lattice parameter and X-ray density of $Ca_xNi_{1-x}Co_2O_4$for*x*=0.0, 0.02, 0.04, 0.06, 0.08, and 0.10.

The X- ray density is given by,

$$\rho = ZM / Na^3 \quad \text{---------- (5)}$$

where, M - molecular weight of the sample, N - Avogadro number.

Fig. 2 shows the variation of lattice parameter and variation of X-ray density as a function of Ca composition(*x*).It was observed that, with the increase in doping concentration, the lattice constant (*a*) increased, it was reported that the variation of lattice parameter depends on the ionic radius of doping ion [23]. In this study the ionic radius of doped $Ca^{+2}$is greater than the ionic radius of host Ni^{+2}ions. The ionic radius of Ni^{+2} and Ca^{+2} in octahedral configuration is 0.69 A^o and 0.99A^o. From XRD analysis, the crystalline size was observed increased, because the diffracted peaks in XRD pattern were shifted to higher diffracted angleswith increase in Ca doping, this is due to the effect of difference between the ionic radius of the doped and host ions, which results in lattice distortion and also effects the width of the diffracted peaks,this increases the crystalline sizewith doping and is consistent with the Debye-Scherer equation.From equation (5), the X-ray density depends on the molecular weight of the sample, in case of calcium its molecular weight is less than the molecular weight of the nickel, therefore the x-ray density values weere observed decreased.

Fig. 3 shows FTIR images of Ca doped $NiCo_2O_4$samples of different doping concentrations. It is used for the analysis of organic and inorganic compounds present in the sample.The IR absorption spectrum is drawn from 400 cm^{-1} to 4000 cm^{-1}. The bond absorbed at 667 cm^{-1} corresponds to bending modes of vibration of cobalt oxide(Co-O) [24]. And bond absorbed at 577 cm^{-1} corresponds to bending modes of vibration of Nickel oxide (Ni-O). The peak observed at 512 cm^{-1} confirms the presence of Ca-O [25], the bond absorbed at 1063 cm^{-1} corresponds to stretching vibrations C-H and C=N, which were appeared due to metal nitrates. The bond observed at 1513 cm^{-1} corresponds to N-O stretching bond.

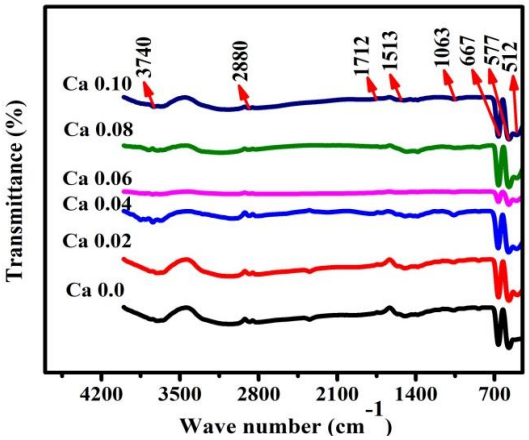

Fig. 3: Fourier Infrared Spectra of Ca doped $NiCo_2O_4$ NPs for *x*=0.0, 0.02, 0.04, 0.06, 0.08, and 0.10.

The bond observed at 1712 cm^{-1} corresponds to C=O stretching vibration mode, the bond appeared at 2880 cm^{-1} is ascribed to the C-H asymmetric stretching mode and other bond positioned at wave number 3740 cm^{-1} is corresponds to O-OH stretching mode, representing the existence of water as moisture [26].

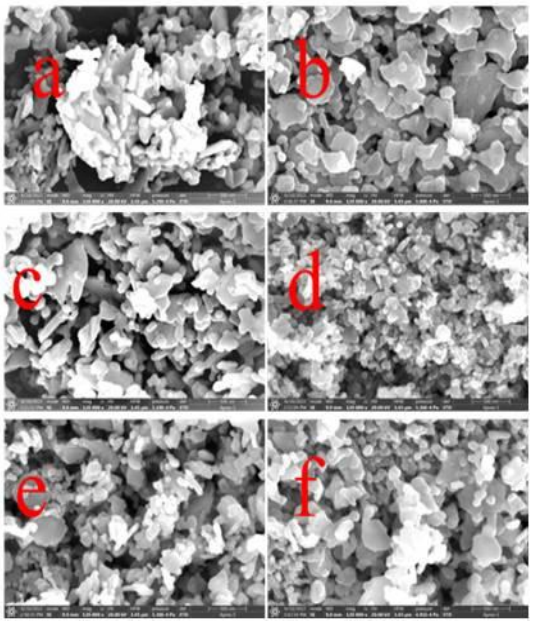

Fig. 4(a-f): FESEM images of Ca doped $NiCo_2O_4$ NPs for *x* = 0, 0.02, 0.04, 0.06, 0.08, and 0.10.

The FESEM was used to study the surface morphology of the sample. Fig. 4, shows FESEM imagesof Ca doped $NiCo_2O_4$ samples at magnification 500 nm, with various Ca doping

concentrations for *x*=0.0, 0.02, 0.04, 0.06, 0.08, and 0.10.

From Fig. 4(a-f), it was observed that the sample surface is formed with hexagonal nanoflake like shape. The sphericalnanoparticles of average grain size in the range of 89 nm(*x* = 0.0) - 143 nm (*x* = 0.10) was observed. From Fig. 4(d) it was noticed that with increase in doping concentration, the grain size was decreased and there is direct relation between grain size and activation energy.As the grain size decreases, the activation energy also decreases [27], therefore the small grain size has low activation energy of the charge transfer and diffusion by which it is easy to take redox reactions and diffusion in electrode material which enhances the electrochemical performance of the material.

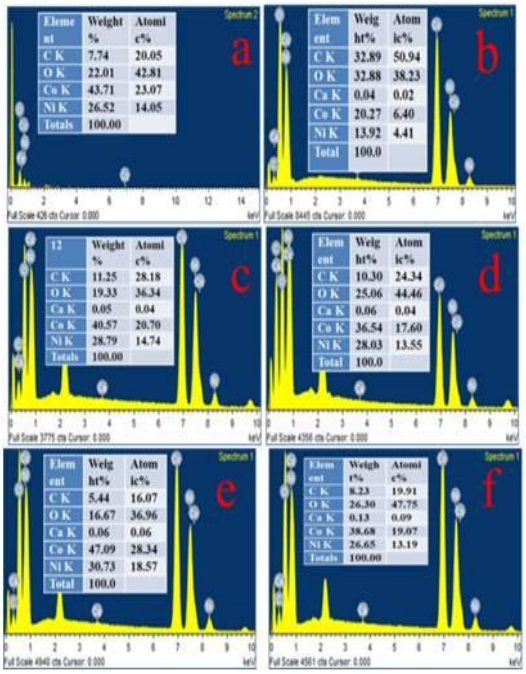

Fig. 5(a-f): EDAX images and elemental compositions of Ca doped $NiCo_2O_4$ NPs for *x* = 0.0, 0.02, 0.04, 0.06, 0.08, and 0.10.

An EDAX study was used to analyze the chemical composition of the sample. The EDAX spectrum is shown in Fig. 5(a-f), from the spectrum it was observed that as per the designed concept, all the elements i.e. Ca, Ni, Co, and O are present in the formation of Ca doped $NiCo_2O_4$ nano particles. The doping elements with their weight and atomic percentage are shown in Fig. 5(a-f).

The XPS study was used to study the energy states of the elements present in the sample. Fig. 6 shows XPS spectra of Ni 2p, Co 2p, Ca 1s and O 1s of the Ca doped $NiCo_2O_4$ samples byusing Gaussian fitting method.

The Fig. 6(a-d) shows the XPS broad spectrum of Ca doped nickel cobalt oxide, in which elements Ca, Ni, Co and O were observed around at binding energies 349.2 eV, 871 eV, 794 eV and 529 eV respectively.

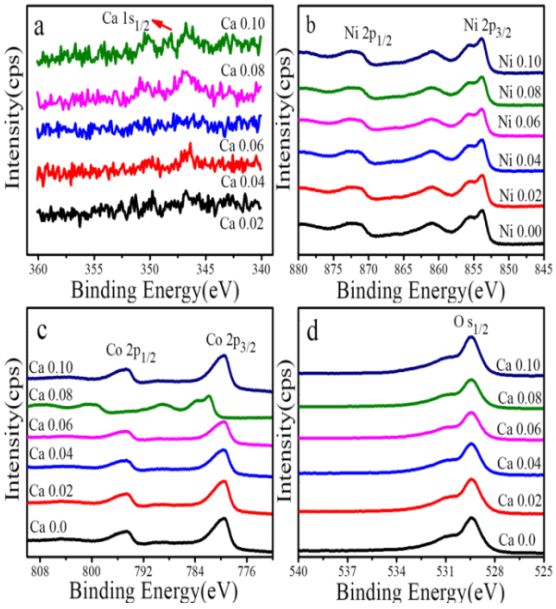

Fig. 6(a-d): X-ray Photoelectron Spectroscopy (XPS) of Ca doped $NiCo_2O_4$ NPs showing the binding energy vs intensity of Ca, Ni, Co and O for *x* = 0.0, 0.02, 0.04, 0.06, 0.08, and 0.10

The cobalt 2p spectrum shown in Fig. 6c, which showstwo spin orbit doublets characteristics [28] of $Co^{2+}$and Co^{3+} with one satellite peak wasobserved.Fig. 6b, shows the Ni 2p spectrum which consists two spin orbit double characteristics of Ni^{2+} and $Ni^{3+,}$ this shows that Ca doped $NiCo_2O_4$nanostructured composition had Co^{2+}, Co^{3+}, Ni^{2+} and Ni^{3+} ions.

The binding energy of Ca $1s_{1/2}$ observed at 349.2 eV can be assigned to Ca-O bond, thebinding energy of Ni $2p_{3/2}$observed at 853 eV can be assigned to Ni-O bond and the binding of Co $2p_{3/2}$observed at 779 eV can be assigned to Co-O bond respectively.

From Fig. 7(a-d), for the sample *x* = 0.06, it was observed that, the Ni 2p spectrum was divided into Ni $2p_{3/2}$ and $Ni2p_{1/2}$ at which the binding energies were observed as 854 eV and 871 eV respectively. Co 2p spectrum was divided into Co $2p_{3/2}$ and Co $2p_{1/2}$ at which the binding energies were observed at 779 eV and 794 eV respectively. The O 1s spectrum showed in Fig. 7(d), confirms the metal oxygen bonding from the peak at 529 eV [29].

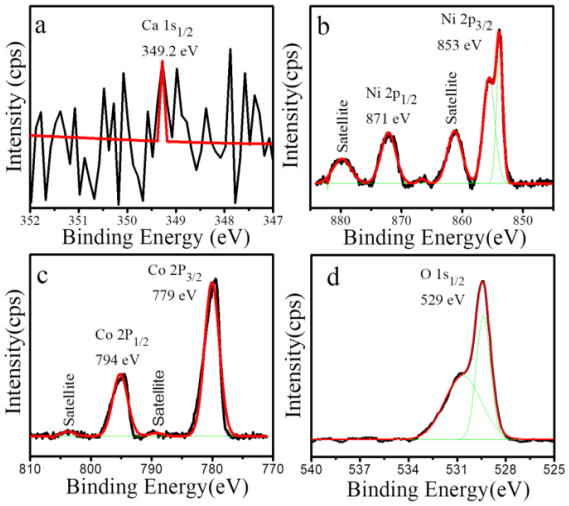

Fig. 7(a-d): X-ray Photoelectron Spectroscopy (XPS) of Ca doped $NiCo_2O_4$NPs showing the binding energy vs intensity of Ca, Ni, Co and O for x = 0.06.

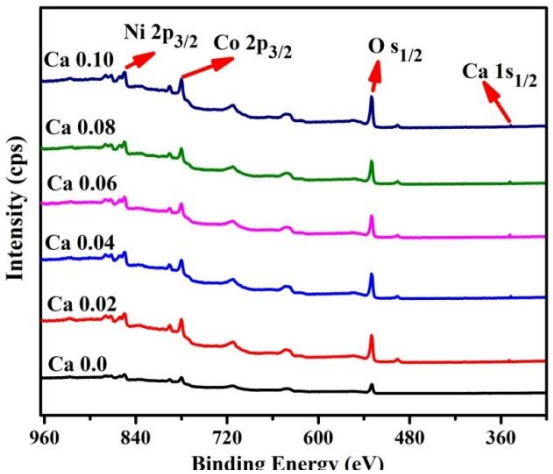

Fig. 8: X-ray Photoelectron Spectroscopy (XPS) of Ca doped $NiCo_2O_4$ NPs showing the binding energy vs intensity of Ca, Ni, Co and O for x = 0.0, 0.02, 0.04, 0.06, 0.08 and 0.10.

Table 2: Showing the binding energies Co, Ni, Ca, and O of Ca doped $NiCo_2O_4$ NPs for x = 0.0, 0.02, 0.04, 0.06, 0.08, and 0.10.

Sl.No	Mg doping, x	Co B.E (eV)		Ni B.E (eV)		Ca B.E (eV)	O B.E (eV)
		$2p_{3/2}$	$2p_{1/2}$	$2p_{3/2}$	$2p_{1/2}$	$1s_{1/2}$	$1s_{1/2}$
1	0.00	779.4	794.6	853.7	871.18	---	529.1
2	0.02	779.4	794.6	853.7	871.8	348.9	530.04
3	0.04	779.6	794.6	853.7	871.5	350.0	530.02
4	0.06	779	794	853	871	349.2	529
5	0.08	781.8	799.6	853.8	872.1	346.6	530.03
6	0.10	779.3	794.6	853.9	871.8	347.2	530.05

From the Fig. 8, it was observed that the binding energy of element Ca is varied in between348.9 eV(x = 0.02) to 347.2 eV (x = 0.10). The binding energy of element Ni is varied in between 871.18 eV (x = 0.0) to 871.8 eV (x = 0.10). The binding energy of element Co is varied in between 794.6 eV (x = 0.0) to 794 eV (x = 0.06). The binding energy of the element O is varied in between 529.1 eV (x = 0.0) to 530.05eV (x = 0.10).

The obtained dielectric data from LCR analyzer explored the dielectric behavior of Ca substituted Nickel cobalt oxide with compositional formula $Ca_xNi_{1-x}Co_2O_4$for x=0.0, 0.02, 0.04, 0.06, 0.08, and 0.10. Fig. 9 shows variation of dielectric constant (k) as a function of frequency (log f) at room temperature. Dielectric constant consists of real and imaginary part, which is given by $K = k' + ik''$, where k' is real part of dielectric constant and k" is the imaginary part of dielectric constant. The dielectric constant is calculated by following formula,

$$K = C / C_o \quad \text{--------} (6)$$

where, Cis the Capacitance of capacitor with dielectric medium and C_o is the Capacitance of capacitor without dielectric medium and is given by,

$$C_o = \varepsilon_o A / d \quad \text{--------} (7)$$

where ε_o denotes thepermittivity of free space, A - denotes the area of pellet, andd - denotes thickness of pellet.

The dielectric constant of the material depends on the number of polarizable groups in the material and the density of the material [30].The dielectric constant of the material is mainly due to different types of polarizations present in the sample. Large number of defects present at the interface of nano crystalline material can cause a change in positive and negative charge distribution, when external field is applied these space charges aligns in the direction of field and causes the formation of dipole moment which is called space charge polarization.

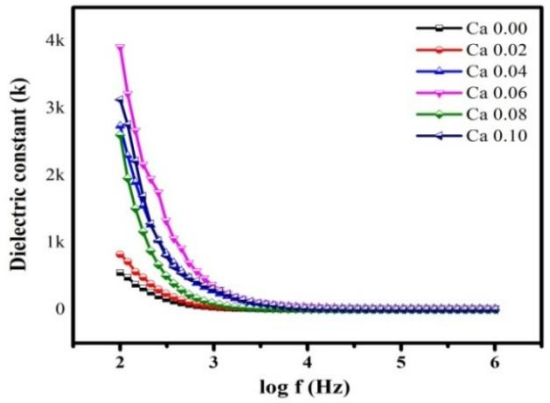

Fig. 9: Dielectric constant (K) vs log f graph of Ca doped $NiCo_2O_4$ NPs for *x*=0.0, 0.02, 0.04, 0.06, 0.08, and 0.10.

Thus, high value of dielectric constant at low frequency is due to this space charge polarization [25]. Fig. 9 shows variation of dielectric constant as a function of logf at room temperature. From the plot it was observed that the dielectric constant had high values in the low frequency region and decreases gradually and become constant at high frequency region. From the plot it was clear that there is a decreasing trend in dielectric constant for all the samples when moved from low frequency region to high frequency region. Koop's theory along with Maxwell's andWagers model [31] explains the decreasing behavior of dielectric constant with increase in frequency. According to this theory at lower frequency, the resistive grain boundaries are more than the conductive grains. Therefore, dielectric constant possesses high values at low frequency region.

The cyclic voltammetry (CV) and Galvanostatic charge and discharge (GCD) test in a conventional three electrode arrangement was performed to analysis the electrochemical behavior of the pure and Ca doped $NiCo_2O_4$ electrode materials with doping concentration *x*= 0.0, 0.02, 0.04, 0.06, 0.08, and 0.10. Using CV, the specific capacitance (C_{sp}) for different scan rates was calculated and by using GCD test, the C_{sp}, energy density (E_d) and power density (P_d) of all electrode materials were calculated.

Fig. 10 (a-e) shows CV curves of Ca doped $NiCo_2O_4$ electrode material for *x* = 0.0, 0.02, 0.04, 0.06, 0.08, and 0.10 at different scan rates 5 mV/s, 10 mV/s, 15 mV/s, 20 mV/s and 25 mV/s respectively. Fig. 10(f) shows the specific capacitance of all Ca doped $NiCo_2O_4$ electrode materials as a function of scan rate. It was observed

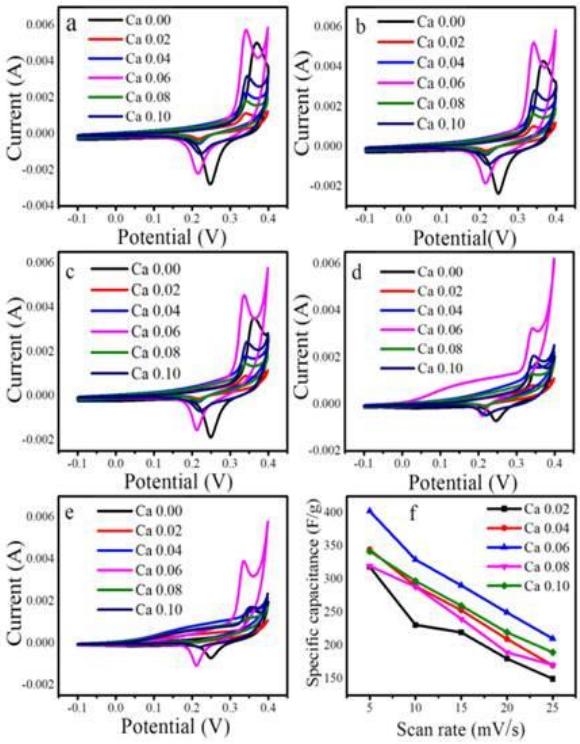

Fig. 10(a-f): Cyclic voltammetry curves of pure and Ca doped $NiCo_2O_4$ electrode materials for *x* = 0.0, 0.02, 0.04, 0.06, 0.08, and 0.10 at scan rates a). 5 mV/s, b). 10 mV/s, c). 15 mV/s, d). 20 mV/s, and e). 25 mV/s respectively and f). Specific capacitance (C_{sp}) vs scan rate.

that among all samples, the electrode material for *x* = 0.06 showed dominant loop area which reveals largest charge storage capacity and higher specific capacitance (C_{sp}).

The specific capacitance is calculated from the CV curves using the formula [32],

$$C_{sp} = \frac{\int I dv}{2\, m V_s \Delta V} \quad F\ g^{-1} \text{ ---- (8)}$$

where, m –denotes mass of active material coated on the electrode (mg), ΔV - the applied potential window and V_s - the scan rate (mVs^{-1}).

Using GCD test, the specific capacitance (C_{sp}), energy density (E_d) and power density (P_d) were calculated by adopting the following expressions [33]:

$$C_{sp} = \frac{I\Delta t}{m\Delta V} \quad F\ g^{-1} \text{ ----- (9)}$$

$$E_d = \frac{1}{2} C_{sp} (\Delta V)^2 \left(\frac{10}{36}\right) \quad Wh\ kg^{-1} \text{ --- (10)}$$

and $$P_d = \left(\frac{Ed}{\Delta t}\right)(3600) \quad W\ kg^{-1} \text{ ---- (11)}$$

where C_{sp}– denotes the specific capacitance of active materials, I - the current applied, Δt - the discharge time duration, m - the mass of active material loaded on Ni foam and ΔV - the applied potential window.

Table 3 shows the specific capacitance of Ca doped $NiCo_2O_4$ electrode materials with doping concentration x = 0.0, 0.02, 0.04, 0.06, 0.08, and 0.10 at different scan rate. From the table it was observed that the specific capacitance decreases with increase in scan rate, because at higher scan rate, faster redox reactions takes place which reduces electrolyte ions diffusion into active material and consequently lowers the capacitance [34].

A grain boundary is the interface between the grains or crystallites in a material, which causes grain resistance and tends to decrease the electrical conductivity of the material. Complex impedance measurement was done for the analysis of grain resistance of Grain boundary regions. Fig. 11, shows Cole-Cole plot drawn between Z' along X-axis and Z" along Y–axis. These graphs provide the information about differentelectro-activeregions. Generally, electro active regions involve the conducting grains, insulating grains and interface boundaries between the samples and electrodes [30]. In this present study one open circle was observed for each sample. From the Fig. 11, it was observed that the diameter of open-circles was decreased and transition was seen from open circle to semi-circle, with the increase in doping concentration.

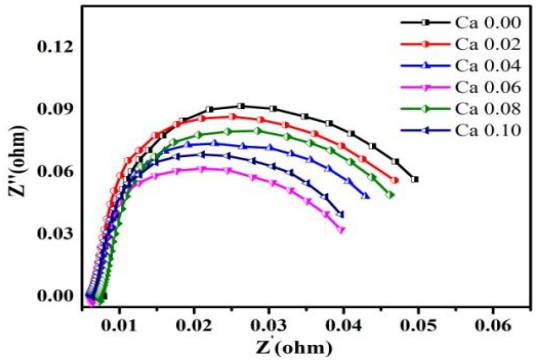

Fig. 11: Cole-Cole (Z'& Z'') graph of Ca doped $NiCo_2O_4$ NPs for x=0.0, 0.02, 0.04, 0.06, 0.08, and 0.10.

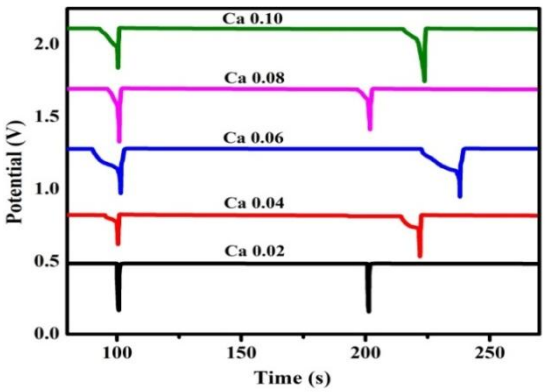

Fig.12: GCD curve of Ca doped $NiCo_2O_4$ electrode material with doping concentration x = 0.0, 0.02, 0.04, 0.06, 0.08 and 0.10.

There is a direct relation between diameter of semi-circle and the resistance of the sample. For x = 0.02, the diameter of semicircle is large, therefore the sample had highly insulating behavior and with increase in doping concentration the diameterof semicircle was decreased and found minimum for x = 0.06, and then increased, which concludes that for the sample x = 0.06, the resistivity is low therefore it possesses high electronic conductivity. From Cole - Cole graph, discussed earlier, it was noticed that the sample with doping concentration x = 0.06, possess low electrical resistance which increases the electrical conductivity of the sample.

The GCD test was performed on pure and Ca doped electrode materials in a potential range from-0.1V to 0.4V in 2M aqueous KOH electrolyte solution at current density 1 Ag^{-1} (i.e., I/m = 1A g^{-1}, where I is the current and m is the mass of the electrode material). Fig. 12 shows the GCD curves of all electrode materials as a function of potential and time. From the figure, the specific capacitance of all the samples were calculated and it was noticed that it increases with increase in doping concentration and is maximum for the sample with doping concentration x = 0.06. However further increase in Ca content results decrease in specific capacitance. The improvement in specific

Table 3: Scan rate and Specific Ca pacitance values (C_p) at different Ca doped $NiCo_2O_4$ NPs for x = 0.0, 0.02, 0.04, 0.06, 0.08, and 0.10.

Sl. No.	Ca Doping x	C_{sp} values (F g^{-1}) at different scan rates				
		5 mV/s	10 mV/s	15 mV/s	20 mV/s	25 mV/s
1	0.02	318.8	231.2	200	180.5	150
2	0.04	344.8	289.8	253.3	210	170.2
3	0.06	402.7	329.6	290.7	250	210.6
4	0.08	319.7	288.7	240.5	190	170.7
5	0.10	342.1	297.2	260.1	220	190

capacitance for the sample x = 0.06 could be attributed to the enhanced electrical conductivity which was illustrated in conductivity part and from the Cole-Cole graph.

The lesser diameter of the semi-circle reveals low resistance therefore the electrode has an easy access to ions for intercalation and de-intercalation. Therefore the highest specific capacitance for the sample x = 0.06 is attributed to the minimum EIS and high electrical conductivity [35].

Table 4 shows the calculated values of specific capacitance (C_{sp}), energy density (E_d) and power density (P_d) of all the electrode materials. From the table it was found that the sample with doping concentration x = 0.06 exhibited a highest specific values of capacitance of 355 F g^{-1}, energy density 10.9 Wh kg^{-1} and power density 235 W kg^{-1} at a current density of 1 Ag^{-1}.

Table 4: Tabulated the energy density (E_d), power density (P_d) and specific capacitance (C_{sp}) values of Ca doped $NiCo_2O_4$ for x = 0.0, 0.02, 0.04, 0.06, 0.08 and 0.10.

Sl. No.	**Mg Doping, *x***	**Discharging time, Δt**	**Potential window ΔV**	**$C_{sp}=\frac{I\Delta t}{m\Delta V}$ (F g^{-1})**	**$E_d = \frac{1}{2}C_{sp}(\Delta V)^2(\frac{10}{36})$ (Wh kg^{-1})**	**$P_d = (\frac{Ed}{\Delta t})$ (3600) (W kg^{-1})**
1	0.0	80	0.33	242	3.66	165
2	0.02	87	0.33	263	3.98	165
3	0.04	114	0.38	300	6.01	190
4	0.06	167	0.47	355	10.9	235
5	0.08	93	0.32	290	4.13	160
6	0.10	85	118	310	6.22	160

IV. CONCLUSIONS

The entire sample formed crystalline with cubic spinel with space group (Fd-3m) and increased with doping of Ca. The formation of hexagonal shaped nanoflakes except for x = 0.06 which are spherical. The dielectric constant of the sample is found highest at lower frequencies for this sample. The GCD studies shows that the highest values of specific capacitance 355 F g^{-1}, energy density 10.9 Wh kg^{-1} and power densities 235 W kg^{-1} at a current density of 1 A g^{-1} for x = 0.06 which is a promising material for the application of electrode for supercapacitor applications.

ACKNOWLEDGEMENTS

The authors are thankful to Prof. D. Karunasagar, Head, Department of Physics, Osmania University for his constant encouragement.

REFERENCES

[1]. J.R. Miller and P. Simon, Electrochemical Capacitors for Energy Management, Science, 321, 2008, 651-652.doi: 10. 1126/science.1158736

[2]. F. El-Kady, V. Strong, S. Dubin and R.B. Kaner, Laser Scribing of High-Performance and Flexible Graphene-Based Electrochemical Capacitors, Science, 335, 2012, 1326 - 1330. doi:10.1126/science.1216744

[3]. Longyan Yuan,Xu Xiao, Tianpeng Ding, Junwen Zhong, Xianghui Zhang, YueShen, Bin Hu, YunhuiHuang, Jun Zhou, and Zhong Lin Wang, Paper-Based Supercapacitors for Self-Powered Nanosystems, Angewand techemie international edition,51, 2012, 4934-4938.https://doi.org/10.1002/anie.201109142

[4]. Yu Wu, Chuanbao Cao, The way to improve the energy density of supercapacitors:progress and perspective,Science China Materials, 61,2018, 1517-1526. https://doi.org/10.1007/s40843-018-9290-y

[5]. Zhong - Shuai Wu , Wencai Ren, Da-Wei Wang, Feng Li, Bilu Liu, Hui- Ming Cheng, High-energy MnO_2 Nanowire/graphene and graphene asymmetric electrochemical capacitors, ACS Nano,4, 2010, 5835-5842.https://doi.org/10.1021/nn101754k

[6]. PravalikaButreddy, SwaroopChakraborty, PushpanjaliSoppina, RakeshBehera, Virupakshi Soppina, Superb K Misra, Novel dual labelled nanoprobes for nanosafety studies: Qualification and imaging experiment if CuO nanoparticles in C. elegans, Chemosphere, 286, 2022, 131698-131706. https://doi.org/10.1016/j.chemosphere.2021.131698

[7]. Wei Chen , R.B. Rakhi, Liangbing Hu, Xing Xie, Yi Cui, H.N. Alshareef, High-

performance nano structured supercapacitor on a sponge,NanoLett,12, 2011, 5165-5172. https://doi.org/10.1021/nl2023433

[8]. JunmingXu, Zhen Han, Jinsong Wu, Kaixin Song, Jun Wu, HuifangGao, YuhongMi, Synthesis and electrochemical performance of vertical carbon nanotubes on few–layer graphene as an anode material for Li–ion batteries,Material Chemistry and Physics, 205,2018, 359-365. https://doi.org/10.1016/j.matchemphys.2017.11.039

[9]. Jiri Libich, Josef Maca, Jiri Vondrak, Ondrej Cech, Marie Sedlarikova, Supercapacitor: Properties and applications, J. Energy Storage, 17,2008, 224–227. https://doi.org/10.1016/j.est.2018.03.012

[10]. Ali Eftekhari, Lei Li, Yang Yang, Poly-aniline supercapacitors, J. Power Sources, 347, 2017, 86–107. https://doi.org/10.1016/j.jpowsour.2017.02.054

[11]. V.C. Lokhande, A.C. Lokhande, C.D. Lokhande, Jin hyeok Kim, TaeksooJi, Super capacitive composite metal oxide electrodes formed with carbon, metal oxides and conducting polymers,Journal of alloys and Compounds, 682, 2016, 381–403. https://doi.org/10.1016/j.jallcom.2016.04.242

[12]. JinleiXie, Ziyue Zhan, ShiweiZhang,Geng Li, Hanchun Xia, Yefeng Yang, JieXiong, $CoMoO_4$ nanoplates decorated $CuCo_2O_4$ nanowires as advanced electrodes for high–performance hybrid supercapacitors, Material Letters, 226, 2018, 30–33. https://doi.org/10.1016/j.matlet.2018.05.017

[13]. Y.F. Yuan, J.X. Lin, D.Zhang, S.M.Yin, Y.L. Zhao, J.L. Yang, Y.B. Chen, S.Y.Guo, Freestanding hierarchical NiO/MnO_2 core–shell nanocomposites arrays for high–performance electrochemical energy storage, 227, 2017, 303–309. https://doi.org/10.1016/j.electacta.2017.01.002

[14]. Chenggang Wang, E Zhou, Weidong He, Xiaolong Deng, Jinzhao Huang, Meng Ding, Xianqi Wei, Xiaojing Liu, XijinXu, $NiCo_2O_4$–based supercapacitor rnanomaterials, Nanomaterial's, 7, 2017, 41. https://doi.org/10.3390%2Fnano7020041

[15]. Cheng Zhang, XinpeiGeng, Shaolong Tang, Mingsen Deng, Youwei Du, $NiCo_2O_4$-rGO hybrid nanostructures on Ni foam as high–performance supercapacitor electrodes, J. Mater. Chem. A,5, 2017, 5912–5919. https://doi.org/10.1039/C7TA00571G

[16]. Guanhua Zhang, Taihong Wang, Xinzhi Yu, Haonan Zhang, HuigaoDuan, BinganLu, Nanoforest of hierarchical Co_3O_4-$NiCo_2O_4$ nanowire arrays for high–performance supercapacitors, Nano Energy, 2, 2013, 586–594. https://doi.org/10.1016/j.nanoen.2013.07.008

[17]. Le Yu, Genqiang Zhang, Changzhou Yuan and Xiong Wen Lou, Heirarchical $NiCo_2O_4$-MnO_2 core shell heterostructurednano wire arrayson Ni foam as high-performance supercapacitor lectrodes, Chem.Commun**,**49**,** 2013**,** 137-139. https://doi.org/10.1039/C2CC37117K

[18]. UmeshT.Nakate and S.N.Kale, Microwave assisted synthesis and characterizationsof $NiCo_2O_4$nanoplates and Electrical, magnetic properties, Material Today:Proceeding, 3,2016, 1992-1998. https://doi.org/10.1016/j.matpr.2016.04.101

[19]. S. Alrousan, B. Albiss, B. Aljawrneh, A. Alshanableh, Amani Al-Othman, H. Megdadi, Nickel-Cobalt oxide nanosheets asymmetric supercapacitor for energy storage applications, Journal of material Science: Materials in Electronics, 34**,**2023**,** 669. https://doi.org/10.1007/s10854-023-10036-2

[20]. Sook-Keng Chang, ZulkarnainZainal, Kar-Ban Tan, Nor AzahYusof, Wan MohamadDaud Wan Yusoff, S. R. S. Prabaharan, Synthesis and electrochemical properties of nanostructured nickel–cobalt oxides as supercapacitor electrodes in aqueous media, International Journal of Energy research,39, 2015, 1366-1377. https://doi.org/10.1002/er.3339

[21]. Kaibing Xu, Wenyao Li, Qian Liu, Bo Li, XijianLiu, LeiAn, ZhigangChen, Ruj iaZou and Junqing Hu, Hierarchical mesoporous $NiCo_2O_4$-MnO_2 core-shell nanowire arrays on nickel foam for aqueous symmetric supercapacitors, J. Mater. Chem.A,2, 2014, 4795-4802. https://doi.org/10.1039/C3TA14647B

[22]. Poonam, Kriti Sharma, Nirmal, S. K. Tripathi, Electrochemical performance of nickel cobalt oxide-reduced graphene oxide-polyvinyl alcohol nanocomposite, AIP Conferenceroceedings, 2220, 2020, 020055**.** https://doi.org/10.1063/5.0001838

[23]. Sumetha Suwanboon, Pongsaton Amornpitoksuk, Apinya Sukolrat, Dependence of optical properties on doping metal, crystallite size and defect concentration of M-doped ZnO nanopowders (M=Al, Mg, Ti), Ceramics International, 37**,** 2011, 1359-

1365.http://dx.doi.org/10.1016/j.ceramint.2010.12.010

[24]. Rohit Raveendran, P.G. Chitra, Optical, Electrical and structural studies of nickel–cobalt oxide nanoparticles,Indian journal of Engineering and Material Science,15, 2008. https://www.researchgate.net/publication/242613358_Optical_electrical_and_structural_studies_of_nickel-cobalt_oxide_nanoparticles

[25]. LulitHabte,NatnaelShiferaw, DureMulatu, ThriveniThenepalli, Ramakrishna Chilakala and JiWhanAhn, Synthesis of Nano-Calcium Oxide from Waste Eggshell by Sol-Gel Method, Sustainabiliti, 11, 2019, 3196. https://doi.org/10.3390/su11113196

[26]. K. Rajasekar, G. Vonod, K. Maesh Kumar, J. LaxmanNaik; Impact of erbium (Er) doping on the structural and magnetic properties Ni-Cu nano ferrites,Journal of Magnetism and Magnetic Materials,555, 2022. http://doi.org/10.1016/j.jmmm.2022.169323

[27]. JiaxinHao, Wenjie Wu, Qiao Wang, de Yan, Guohan Liu and Shanglong Peng, Effect of grain size on Electrochemical Performance and Kinetics of Co_3O_4 electrode material, J. Mater.Chem, 8, 2020, 7192-7196. https://doi.org/10.1039/D0TA02032J

[28]. Ai-Lan Yan, Wei-Dong Wang, Wen-Qiang Chen, Xin-Chang Wang, Fu Liu and Ji-Peng Cheng, The synthesis of $NiCo_2O_4$-MnO_2 core shell nanowires by Electro-deposition and its Supercapacitive Properties, Nano Material, 9**,** 2019, 1398. doi:10.3390/nano9101398

[29]. P. Butreddy, H. Holden, H. Rathnayake, Macromol, Metal ion-Directed coordination programming of biomolecules to bioinspired nanoflowers, Chem. Phys,223, 2022, 2200237-2200243. http://doi.org/10.1002/macp.202200237

[30]. Sujoy Saha, Sheeba Dawood, Pravalika Butreddy, GayaniPathiraja and Hemali Rathnayake, Novel biodegradable low-k dielectric nanomaterials from natural polyphenols, RSCAdv, 11, 2021, 16698-705.https://doi.org/10.1039/D1RA01513C

[31]. Muhammad Mubashar Munir, Ali Raza Khan, Ghulam M Mustafa, S. Kumail Abbas, M.AkramRaza, ShahidAtiq, Shahazad Naseem, Dielectric and magnetic variance $NiCo_2O_4$spinel's mediated by Zn-substitution for efficient data and energy storage, Applied physics, 127, 2021, 492. http/doi.org/10.1007/s00339-021-04640-4

[32]. R. Roshani, A. Tadjarodi, Synthesis of $ZnFe_2O_4$ nanoparticles with high specific surface area for high-performance supercapacitor, J. Mater. Sci. Mater. Electron, 31, 2020, 23025–23036. DOI:10.1007/s10854-020-04830-5

[33]. D.P. Dubal, G.S. Gund, C.D. Lokhande, R. Holze, CuO cauliflowers for supercapacitor application: Novel potentio-dynamic deposition,Mater. Res. Bul, 48, 2013, 923-928.https://doi.org/10.1016/j.materresbull.2012.11.081

[34]. Shahrzad Arshadi Rastabi, Rasoul Sarraf-Mamoory, Ghadir Razaz, Nicklas Blomquist, Magnus Hummelgard, Hakan Olin, Treatment of $NiMoO_4$-nanographite nanocomposite electrodes using flexible graphite substrate for aqueous hybrid supercapacitors, 16**,** 2021**,** 0254023. DOI**:**10.1371/journal.pone.0254023

[35]. Xiaobo Chen, Cheng Chen, Tianzhi Xu, Yingjie Xu, Weiwei Liu, Wen Yang and Peizhi Yang, performance enhancement of asymmetric super capacitors with bud–like Cu doped Mn_3O_4 hollow and porous structures on nickel foam as positive electrodes, RSC Adv**,** 8, 2018, 35878-35887.https://doi.org/10.1039/C8RA06989A.